Template Assisted Preparation of High Surface Area Macroporous Supports with Uniform and Tunable Nanocrystal Loadings

Michael T.Y. Paul, Brenden B. Yee, Xin Zhang, Eiji H. Alford,

Brandy K. Pilapil, and Byron D. Gates*

*bgates@sfu.ca

Department of Chemistry, Simon Fraser University

8888 University Drive, Burnaby, B.C. V5A 1S6, Canada

Final version published as: "Template Assisted Preparation of High Surface Area Macroporous Supports with Uniform and Tunable Nanocrystal Loadings," Paul, M. T. Y.; Yee, B. B.; Zhang, X.; Alford, E. H.; Pilapil, B. K.; Gates, B. D., *Nanoscale*, 2019, 11, 1937-1948. DOI: 10.1039/C8NR07762B

Abstract

The incorporation of catalytic nanocrystals into macroporous support materials has been very attractive due to their increased catalyst mass activity. This increase in catalytic efficiency is attributed in part to the increased surface area to volume ratio of the catalysts and the use of complementary support materials that can enhance their catalytic activity and stability. A uniform and tunable coating of nanocrystals on porous matrices can be difficult to achieve with some techniques such as electrodeposition. More sophisticated techniques for preparing uniform nanocrystal coatings include atomic layer deposition, but it can be difficult to reproduce these processes at commercial scales required for preparing catalyst materials. In this study, catalytic nanocrystals supported on three dimensional (3D) porous structures were prepared. The demonstrated technique utilized scalable approaches for achieving a uniform surface coverage of catalysts through the use of polymeric sacrificial templates. This template assisted technique was demonstrated with a good control over the surface coverage of catalysts, support material composition, and porosities of the support material. A series of regular porous supports were each prepared with a uniform coating of nanocrystals, such as $NaYF_4$ nanocrystals supported by a porous 3D lattice of $Ti_{1-x}Si_xO_2$, Pt nanocrystals on a 3D porous support of TiO_2, Pd nanocrystals on Ni nanobowls, and Pt nanocrystals on 3D assemblies of Au/TiO_2 nanobowls. The template assisted preparation of high surface area macroporous supports could be further utilized for optimizing the use of catalytic materials in chemical, electrochemical, and photochemical reactions through increasing their catalytic efficiency and stability.

Introduction

This study describes a series of methods for creating uniform and tunable coatings of nanocrystals supported on the surfaces of custom built macroporous materials with two dimensional (2D) or three dimensional (3D) structures. These techniques can be used to prepare supports with a desired porosity, catalytic activity, and chemical stability. Catalytic nanocrystals are widely utilized in chemical reactions due to the significant increase in surface area to volume ratio of these systems relative to larger particles or agglomerates.[1–3] This increased surface area to volume ratio can improve the catalyst mass activity, increase catalyst utilization, and reduce the cost of the systems that incorporate these nanocrystals.[4–6] Systems designed for the generation of renewable energy, which include proton exchange membrane fuel cells (PEMFCs) and direct methanol fuel cells (DMFCs), utilize nanocrystals such as Pt and Pd.[4–7] To optimize the delivery of reagents to and removal of products from these or similar catalytic systems, materials can be prepared with a tunable porosity using pore forming agents or templates. The preparation of inverse opaline (IO) structures provides access to ordered, close-packed, and interconnected pores, which have been pursued for both fundamental studies in fluid dynamics and an enhanced performance as porous electrodes.[8,9] For example, cathode electrodes in PEMFCs composed of Pt IOs can improve the oxygen reduction reaction (ORR) activities.[10,11] This improvement in catalyst efficiency was attributed to the macroporous IO structure for its influence on the mass transport of reactants and products to and from the surfaces of this catalyst.[10,12–15] The current study seeks to extend this knowledge by demonstrating a series of different types of nanocrystals coated onto the surfaces of various support materials each with a targeted morphology. The morphologies pursued here include IOs, dimpled surfaces, and randomly packed nanobowls. These studies demonstrate methods to create a variety of

macroporous supports that incorporate uniform and tunable coatings of nanocrystals, which enables the targeted material to be adjusted to the needs of the intended catalytic reaction.

Many studies have indicated the composition of support materials can improve the electrochemical activity and thermal stability of the supported nanocrystals. These synergistic effects have been observed for a variety of materials through strong metal-support interactions.[16,17] Currently, the loading of nanocrystals onto surfaces of a structured support is often performed by nanocrystal powder processing, nanocrystal suspension/solution casting, electrodeless and electrochemical deposition techniques, and atomic layer deposition (ALD) methods.[13,14,18–20] Powder processing and solution casting of nanocrystals are often used to achieve uniform, planar coatings of materials. These techniques may, however, result in the formation of nanocrystal agglomerates due to the of processing conditions.[18,21] This agglomeration can reduce the overall mass efficiency of the nanocrystals by reducing their surface area to volume ratio.[14,18] Macroporous materials can be created to replace powder based catalyst supports to reduce the possible aggregation of the nanocrystals. It is, however, difficult to coat the inner surfaces of a 3D macroporous support with nanocrystals by powder processing and solution casting techniques.[22–24] For improving the uniformity of nanocrystal coatings in macropores, electrochemical deposition can be used to prepare nanocrystals that exhibit limited agglomeration and increased mass efficiency.[25–27] This technique is limited to precious metal based support materials because the solutions used for the electroless and electrodeposition of precious metal catalysts are typically corrosive to lesser noble metals through processes of galvanic replacement.[20,23] Solutions of Pd and Pt salts for these processes are often prepared at a low pH to improve their stability.[23] The low pH of these electroless and electrodeposition processes can easily damage the nano- and microscale features of a macroporous support

prepared from lesser noble metals. Furthermore, electrodeposition can result in a relatively non-uniform deposition of material within a 3D macroporous support due to diffusion based limitations imposed by concentration gradients, proximity of neighboring deposition sites, and shape of the electric field lines.[27] For improving the uniformity of nanoscale catalysts within 3D macroporous supports, techniques such as ALD can be used for effectively infiltrating metal precursors into the pores.[13,19] This deposition technique is, however, very time consuming. A deposition rate of 1 to 2 nm of material per hour is commonly observed, but it can be as slow as <1 nm/h.[13] These relatively long processing times, the relatively small sample sizes, and the necessity to place the support materials under vacuum during this process, make ALD a relatively expensive technique in comparison to the other aforementioned methods. As mentioned previously, the characteristics of nanocrystals can be enhanced or complemented by the presence of the support material or the interface between the catalyst particles and the supports. For example, niobium oxide or silicon dioxide supported Pt nanocrystals can exhibit improved electrochemical or thermal stabilities, respectively.[28,29] In a second example, the (117) facet of an α-$(NiCu)_2Pd$ alloy can achieve three times the catalytic activity of the Pd (111) facet.[30] Catalytically active alloys, such as these can be formed at the interface between a nanocrystal and its support.[10,16] To take advantage of these interactions between nanocrystals and their supports requires alternative processing methods. It is also desired that these methods can overcome nanocrystal agglomeration, non-uniform coverage of the supports, and to address other challenges with processing these materials. A series of relatively simple methods are discussed here that can achieve a uniform surface coverage of nanocrystals within 2D and 3D macroporous supports. These methods are scalable, compatible with a variety of materials, and utilize relatively mild processing conditions.

Nanocrystals of a range of compositions were loaded onto the surfaces of macroporous supports while achieving both a uniform interparticle spacing, a tunable loading of catalyst particles, and controlled interactions between the nanocrystals and their support. Compositions of the support materials were also tuned to demonstrate the preparation of macroporous metals, semiconducting metal oxides, and insulating ceramics. Our preparation technique combined the assembly of these nanocrystals onto spherical sacrificial templates, the self-assembly of nanocrystal covered templates, the formation of a support matrix within the interstitial spaces among the assembled templates, and the selective removal of the sacrificial templates to create the macroporous products. The self-assembly of nanocrystals onto spherical templates was previously demonstrated, but with limited success in controlling the uniformity of the loading, and extending the process to a diverse range of materials.[31,32] These procedures have been fine tuned to prepare uniform loadings of nanocrystals on the surfaces of spherical polymer templates while also achieving a tunable surface coverage.[12,15,33] These processes relied on controlling the surface chemistries of both the nanocrystals and the polymer spheres. The refined process was used here to coat nanocrystals of different sizes, shapes, and compositions onto polymer spheres with uniform and tunable surface coverages. These coatings included nanocrystals of $NaYF_4$ (diameter, ø = 26 ± 4 nm), Pt (ø = 3.4 ± 0.5 nm), and Pd (ø = 13 ± 2 nm), which were chosen for their desirable catalytic properties and/or their utility in the generation of renewable energy.[4–6]

To create the macroporous materials, with average pore diameters of 1 μm to 50 nm, in this study, nanocrystal coated polymeric templates were self-assembled into ordered arrays with similar procedures that have been previously pursued for creating photonic band gap materials.[8,34,35] Spherical templates coated with either the $NaYF_4$, Pt, or Pd nanocrystals were used here to create macroporous supports whose inner surfaces were uniformly covered with

nanocrystals. The nanocrystal coated spherical templates were first organized into close-packed arrays by self-assembly at an air-water interface. These close-packed layers of the templates were lifted from the air-water interface in a finely controlled, layer-by-layer fashion, to produce 2D or 3D crystalline assemblies.[10] The formation of ordered support matrices was achieved by infiltrating the interstitial spaces among these assembled templates with the desired precursors. For example, metal alkoxide solutions or solutions of metal salts were used for the formation of metal oxides by sol-gel techniques or the preparation of metals by electrodeposition, respectively.[10,11,20,36] The support materials deposited or grown around the nanocrystal coated templates can partially encapsulate the nanocrystals and immobilize them within the support matrix. After the nanocrystals were partially immobilized in the support, the polymer templates were selectively removed by thermal degradation or solvent dissolution to create the macroporous supports coated with uniform layers of nanocrystals. Macroporous supports with randomly arranged interconnecting pores were also prepared using the same spherical templates. Nanobowls were created by physical vapor deposition (PVD) of thin film(s) onto assemblies of the polymer templates followed by the selective removal of these templates and subsequent assembly of the isolated bowls into randomly packed structures.

A range of support materials were created in this study, each prepared by a different technique as a demonstration of the versatility of this approach to produce nanocrystal coated macroporous supports. The techniques to deposit or grow the support materials included PVD, electrodeposition, and sol-gel processes for preparing metal and metal oxide films, metallic matrices, and metal oxide matrices, respectively. The diameters of the templated features were precisely controlled through the choice of templates (e.g., diameter of the spherical polymer templates). The diameter of the pores, surface coverage of nanocrystals, and other structural

features within the supports were confirmed by scanning electron microscopy (SEM), transmission electron microscopy (TEM), and energy dispersive X-ray spectroscopy (EDS) techniques. These studies demonstrated a series of approaches to preparing and tuning structural supports coated with nanocrystals. The resulting materials can have tuned chemical, electrochemical, and photochemical properties, including an increased catalytic efficiency and improved chemical, electrochemical, and thermal stabilities. A precise control over the thickness and porosity of the support, the composition of the support and its nanocrystals, and surface coverage of these nanocrystals will enable researchers to tune and optimize the formation of macroporous catalytic materials for an array of applications.

Experimental

Experimental Overview

The general procedure for preparing macroporous supports with uniform coatings of nanocrystals involved the following four steps: (1) preparation of nanocrystal loaded onto spherical polymer templates; (2) self-assembly of these spherical templates; (3) deposition or growth of support materials within these assembled templates; and (4) selective removal of the sacrificial polymer templates. Schematic depictions of the three types of porous structures that were prepared in this study are shown in Figure 1. Detailed procedures for their preparation are outlined below.

Preparation of Nanocrystal Coated Spherical Polymer Templates

The preparation of nanocrystals supported in a 2D or 3D porous matrix began with the coating of nanocrystals onto spherical colloidal templates. Polyvinylpyrrolidone surfactant

stabilized (M_w ~55,000; Sigma-Aldrich, USA) Pt and Pd nanocrystals were each synthesized by a hydrothermal process.[37,38] The $NaYF_4$ photon upconverting nanocrystals were prepared via a thermal decomposition method.[39] The procedures for coating these nanocrystals onto polymer spheres were adopted from previously published methods.[12,15,33] A variety of nanocrystals with a range of compositions and diameters can be coated onto spherical polystyrene (PS) templates (Polybead® Amino Microspheres, Polysciences, Inc., UK). The coating process involved tuning the interactions between the spherical templates and the nanocrystals. Attractive interactions between the nanocrystals and templates included a combination of van der Waals and electrostatic interactions.[31] By preparing nanocrystals with complementary surface charges or surface energies, nanocrystals of different compositions and sizes can be uniformly coated onto the spherical templates. A precise control over the nanocrystal coatings on the templates can be used to tailor their composition as needed for various catalytic applications. For example, Pt nanocrystals can be incorporated with their dimensions optimized for the ORR in PEMFCs, and Pd nanocrystals can be incorporated that are optimized for catalyzing methanol oxidation in DMFCs.[4–6] In the subsequent step, spherical polymer templates with uniform coatings of these nanocrystals were self-assembled into 2D or 3D ordered lattices.

Self-Assembly of Nanocrystal Coated Spherical Templates

The assembly of nanocrystal coated spherical templates into an ordered structure is desirable for producing matrices with interconnecting pores of regular dimensions, and for the preparation of structurally sound porous supports. The morphology, pore dimensions, and thickness of the final form of these porous materials can be adjusted as required by the desired application, such as for their influences on the mass transport of reactants and products in

catalytic processes. The nanocrystal coated polymer spheres can be assembled into ordered lattices by a variety of techniques as demonstrated in previous literature.[12,33,40–45] These self-assembled templates can range from monolayers of hexagonally close-packed spheres to ordered multilayer assemblies. In this study, hexagonally close-packed monolayers were obtained by assembling the nanocrystal coated templates at an air-water interface, followed by selectively transferring these assemblies to a planar substrate.[10] This procedure can be repeated as necessary to prepare multiple layers of the close-packed templates in a finely controlled manner. For a faster process of self-assembly when preparing multi-layered crystalline templates, convective evaporation was also used for preparing relatively thick layers of self-assembled nanocrystal coated templates.[43,45–47] The interstitial spaces within the assembled arrays of spherical templates, with their homogeneous coatings of nanocrystals, were subsequently infiltrated with support materials by vapor or solution-phase techniques. The creation of a solid support matrix surrounding the templates resulted in the immobilization of the nanocrystals and the formation of a bicontinuous network of support materials and sacrificial templates.

Support Material Preparation and Template Removal

Support materials were deposited onto, or grown within the interstitial spaces of the templates. These materials covered the surfaces of the templates, immobilized the nanocrystals, and created stable structures that supported the nanocrystals within a macroporous framework after the removal of the polymeric templates.[10,40,47] Removal of the polymer templates generated either 3D porous structures or textured surfaces with nanoscale relief features. In this study, three strategies were used to prepare structured porous support materials with final compositions ranging from metals, to semiconducting metal oxides, to insulating ceramics. Details of the

specific techniques used to prepare these materials, along with the corresponding methods for template removal are provided in the following sections.

1) Sol-Gel Formation of Porous Supports — 3D $Ti_{1-x}Si_xO_2$ Supported $NaYF_4$ Nanocrystals

A multilayered 3D porous matrix of $Ti_{1-x}Si_xO_2$ supporting a uniform coating of $NaYF_4$ nanocrystals were prepared by sol-gel processing. Ordered assemblies of spherical PS templates coated with $NaYF_4$ nanocrystals were prepared on polished Si (International Wafer Service Inc.; N_p <100>) wafers using convective evaporation techniques.[8,40] The nominal diameters, as determined by TEM, of the $NaYF_4$ nanocrystals and that of the PS templates were ~26 nm and ~320 nm, respectively. The sol-gel process began with spin casting multiple aliquots of a dilute sol-gel solution over the ordered assemblies of the nanocrystal coated polymer spheres. The spin casting method allowed a thin layer of sol-gel solution to be deposited within the interstitial spaces of the assembled templates. Multiple coatings of the dilute solution were used to improve the uniformity of the coatings. The sol-gel coated sacrificial templates were thermally treated to sinter the metal oxide precursors and to create a continuous structural support, as well as to decompose the polymer templates and to isolate the desired porous structure. The sol-gel recipe was modified from a previously reported method to prepare films of TiO_2.[48] In this study, a TiO_2/SiO_2 sol-gel solution was prepared with 1.6 mL of trifluoroacetic acid (TFA; reagent grade, Caledon Laboratory Chemicals, Canada), 2 mL of titanium (IV) ethoxide (99.5%, Sigma-Aldrich, United States), and 0.4 mL of HCl (36.5 to 38%, high purity, ACP Chemicals, Canada). This mixture was shaken for 20 min, followed by the addition of 1 mL of tetraethylorthosilicate (TEOS, 98%, Sigma-Aldrich, United States). This final mixture was diluted 150 fold by volume with anhydrous ethanol (Commercial Alcohols, Canada). The dilute sol-gel solution was spin

cast over 800 rpm, for 1.5 min per step (Brewer Science, United States) onto the ordered assemblies of $NaYF_4$ nanocrystal coated polymer spheres. A 10 μL aliquot of the sol-gel solution was drop cast with each step, and a total of 20 aliquots were cast onto the substrates to ensure an even and optimal coverage of the sol-gel solution within the interstitial spaces of the assembled templates. The sol-gel coated templates were subsequently heated while exposed to air in a furnace (Model 48000 Furnace, Barnstead Thermolyne, United States) at 450 °C to sinter the mixture of silica and titania, as well as to thermally decompose the templates and isolate the macroporous supports. The heating ramp rate was 112.5 °C/h, with a 48 h dwell at 450 °C, and a slow cool down to room temperature over at least 6 h. These samples were directly characterized by a series of techniques including focused ion beam (FIB) milling and selective lift-out of thin sections of the sample for further analysis by TEM techniques.

2) Sol-Gel Formation of Porous Supports — 3D Porous Network of TiO_2 Supported Pt Nanocrystals

Ordered porous TiO_2 supports coated with Pt nanocrystals were prepared in a similar manner as the ordered porous TiO_2/SiO_2 supports for the $NaYF_4$ nanocrystals. A series of spherical PS templates were coated with an increasing surface coverage of Pt nanocrystals. The surface coverage of Pt nanocrystals was controlled by dilution of the Pt nanocrystals relative to the concentration of PS templates in solution during the preparation of the nanocrystal coatings. Three different mixtures were prepared: (i) a relatively low surface coverage from a 90 v/v % diluted solution; (ii) a medium surface coverage from a 60 v/v % diluted solution; and (iii) a relatively high surface coverage from an undiluted, as-synthesized solution of nanocrystals. This study sought to determine if the coverage of nanocrystals in the resulting macroporous matrices

corresponded to the initial nanocrystal loadings on the PS templates. All other preparations were identical to the procedures for creating the ordered porous TiO_2/SiO_2 supports of $NaYF_4$ nanocrystals, except that the TiO_2 sol-gel solution was prepared without the addition of TEOS. Once the porous materials were obtained after the high temperature treatment, the samples were physically fractured, and removed from the surfaces of the polished Si wafer through the use of a razor blade. The fragments from the sample were collected in a centrifuge tube containing 100 μL of DI water (18 MΩ·cm) , and 10 μL of this suspension was drop cast onto a Formvar/carbon coated TEM grid and dried overnight under ambient conditions (01753-F, Formvar/carbon support film, Ted Pella Inc., United States).

3) Electrodeposition of Dimpled Supports —Hexagonally Close-packed Arrays of Dimpled Ni Supporting Pd Nanocrystals

Hexagonally close-packed arrays of dimpled features in Ni with the surfaces of these recessed features coated with Pd nanocrystals were prepared by self-assembly and electrodeposition methods. To prepare these ordered arrays of Pd nanocrystals supported on dimpled Ni, a single close-packed layer of PS templates coated with the Pd nanocrystals were prepared by assembly at an air-water interface followed by transfer to a piece of Ni coated Si wafer. The 150-nm thick Ni (99.98% Ni pellets purchased from Kurt J. Lesker, United States) was deposited by thermal evaporation onto 10 nm of Cr (99.95% Cr pellets purchased from Kurt J. Lesker, United States) that served as an adhesion layer between the Si wafer and the Ni coating. These materials were deposited using a custom built thermal evaporator in 4D LABS at SFU. The template coated Ni substrate was air dried and used as the working electrode in a two-electrode setup for electroplating of Ni (Bio-Logic Science Instruments SP150, United States). A

platinum wire (0.6-mm diameter, 99.98% Pt, Alfa Aesar, United States) was used as the counter electrode. The electrodes were immersed in a Watts plating bath solution (Transene Company, United States) and Ni was electrochemically deposited within the voids of the polymer templates at a current density of ~0.3 A/cm^2 for 1 min. The extent of Ni deposition and the final structure of the arrays were verified by SEM prior to template removal. After Ni electrodeposition, the PS template was selectively removed by Soxhlet extraction with a 50:50 (v/v) mixture of toluene and acetone for at least 12 h. The arrays of dimpled Ni coated with Pd nanocrystals were evaluated using electrochemical techniques, as well as electron microscopy based analyses.

4) Physical Vapor Deposition of Nanobowl Supports — Random Assemblies of Au/TiO_2 Nanobowls Covered with Pt Nanocrystals

Random assemblies of nanobowls were created using PVD of metal or metal oxide thin films on top of assemblies of Pt nanocrystal coated polymer spheres. Close-packed monolayers of Pt coated PS templates were assembled on polished Si substrates. These self-assembled structures were dried overnight in a vacuum desiccator to remove residual moisture. The template coated substrates were loaded into a Kurt J. Lesker PVD 75 system, and 20 nm of TiO_2 (99.9% purity, 3" diameter x 0.125" thick sputter target, purchased from Kurt J. Lesker) was deposited on top of the assembly using radio frequency (RF) sputtering. This TiO_2 coated sample was transferred to another PVD 75 system for the deposition of 20 nm of Au (99.9990% purity, 1/8" evaporation pellets, purchased from Materion) by electron beam (e-beam) evaporation. The PS templates coated with this multilayer film were removed from the substrate by ultrasonication while immersed in a 20 mL glass scintillation vial containing 10 mL of a 50:50 (v/v) toluene to acetone solvent mixture. The suspension was transferred into a 100 mL round bottom flask and

more of this solvent mixture was added to bring the total solution volume to 20 mL. This suspension of polymer spheres with the TiO_2, Au, and Pt nanocrystal coatings were heated to reflux, and the reflux maintained for a total of 5 h. This solution was decanted and fresh solvent added every 60 min during this selective removal of PS templates. The suspension of nanobowls was purified twice with ethanol (centrifugation at 10,000 rpm for 10 min, decanting the supernatant, adding fresh solvent, sonicating for 5 min, and repeating this process) and twice again with water (i.e., repeating the same purification process). A portion of these suspensions were drop cast onto a Formvar/carbon coated TEM grid for analysis by TEM. Another portion of the sample was prepared by mixing the purified sample with 100 μL of Nafion® DE2020 solution (20 wt/wt %, Dupont, United States) and drop cast onto a substrate for focused ion beam milling to prepare cross-sections that were analyzed by SEM.

Details of the Electron Microscopy Characterization

Electron microscopy techniques, such as SEM and TEM, were used at each stage of the sample preparation for: (i) verifying the loading of nanocrystals on the PS templates; (ii) verifying the assemblies prepared from the nanocrystal coated polymer spheres; (iii) verifying the deposition or growth of the support materials; and (iv) identifying the structural morphology and elemental composition of the final material after removal of the polymer templates. The SEM analyses were performed using an FEI Helios NanoLab 650 SEM/FIB dual beam system operating at 5 kV for imaging samples with the presence of polymeric materials and at 10 kV for samples without polymers. Cross-sections of some samples were prepared using a focused Ga ion beam (Tomahawk™ ion column). Layers of platinum with a thickness of ~ 500 nm to 1 μm were deposited onto the samples as a protective coating prior to ion milling to preserve the

surface morphology of the samples. An acceleration voltage of 30 kV was used for the FIB milling and lift-out of a lamella of the sample of interest. The lifted lamella was attached to a lift-out TEM grid (Omnigrid®, Tedpella, USA) with ion beam deposited Pt. The lamella was thinned with a 16 kV FIB to a final thickness of ~ 50 nm. These lifted sections were further analysis by TEM. Sections measuring about 4 μm in length by 1 μm in depth and with a width of ~100 nm were milled, lifted from the samples, and transferred onto the lift-Out TEM grids for analysis by TEM, scanning TEM (STEM), and EDS. All of the TEM related analyses were performed using an FEI Osiris X-FEG S/TEM operating at 200 kV. The EDS analyses were performed with a Super-X EDS detection system as a part of the TEM analysis.

Results and Discussion

In this study, a series unique macroporous structures were prepared using different combinations of support materials and nanocrystals. These materials were created using techniques that included: (i) preparation of nanocrystal coated spherical polymer templates; (ii) self-assembly of these spherical templates; (iii) deposition or growth of support materials onto, or within these assembled templates; and (iv) selective removal of the sacrificial polymer templates. The resulting materials included ordered 3D macroporous supports with $NaYF_4$ particles for optoelectric applications, regular 3D macroporous supports with Pt particles for chemical and photochemical catalysis, arrays of dimpled supports with Pd particles for applications in DMFCs, and random assemblies of nanobowl supports with Pt particles for flow-through catalytic applications. These methods enable a range of tunable parameters, such as adjusting the composition and surface coverage of nanocrystals, as well as altering the composition, pore diameter, structural morphology, and overall thickness of the macroporous supports. These materials can be adjusted as needed to optimize their performance for specific

purposes. For example, the loading densities of nanocrystals and porosity of the support can be simultaneously tuned for their influence on mass transport of reagents and products, and the overall catalytic efficiency.[11,27,49] Each set of materials were analyzed by a series of electron microscopy techniques to verify their porosity, surface coverage of nanocrystals, and material compositions.

Ordered Macroporous Supports for Photocatalytic Applications

Ordered macroporous $Ti_{1-x}Si_xO_2$ supports coated with $NaYF_4$ nanocrystals were prepared for photocatalytic applications. The presence of $NaYF_4$ nanocrystals can enhance the photocatalytic activities of the mixed TiO_2 and SiO_2 porous support material.[50–53] The sol-gel technique for preparing the porous oxide supports is described in the experimental section. A thin section of this sample was lifted out with assistance by FIB milling and analyzed by TEM. The structure of the macroporous $Ti_{1-x}Si_xO_2$ supports for the $NaYF_4$ nanocrystals is shown in Figure 2 with the corresponding EDS spectrum presented in Figure S1. This section of the multi-layered porous metal oxide portrays the ordered structure containing pores with uniform diameters of 320 ± 30 nm. The structures contained interconnected pores within a 3D framework. The high angle annular dark field (HAADF) STEM analyses of the sample indicated the presence of nanocrystals composed of higher atomic number elements that were supported by the oxide matrix. The position of these nanocrystals was further confirmed by EDS mapping, which resolved the atomic composition of elements within these macroporous supports. The overlaid EDS map with the HAADF-STEM image indicated the presence of Y at discrete locations, indicating the successful transfer of the $NaYF_4$ nanocrystals from the polymer templates onto the sintered oxide support.

Recent studies have used $NaYF_4$ nanocrystals supported on TiO_2 nanocrystals for improving their photocatalytic performance.[50] It has also been shown that by using TiO_2 as a support for these upconverting nanocrystals, their emission intensities can be enhanced by more than five times.[54] These enhancements in upconversion efficiency can be further utilized by dye sensitized solar cells, where improvements in the efficiency of up to 37% have been demonstrated for converting solar radiation to electrical power by utilizing TiO_2 supported upconverting nanocrystals along with photosensitive dyes.[55] Future studies may utilize the tunable macroporous framework, such as that depicted in Figure 2, for either accommodating photosensitive dyes within its open lattice for further improving its solar conversion efficiencies or as an open porous support for seeking enhanced photocatalytic materials. The ordered arrays of textured surfaces prepared in this study, with features that ranged from ~30 nm to 300 nm, could exhibit plasmonic and anti-reflective properties across the visible light spectrum that can further improve photovoltaic efficiencies of the supported materials.[7,56] Future investigations may utilize the methods outlined in this study for preparing photocatalytic or otherwise photosensitive materials with precisely tuned surface features, porosity, and composition to optimize their optical properties. The techniques demonstrated in this study provide a platform for preparing high surface area materials with a fine tuned and uniform surface coverage of cataytically and/or optoelectronically active nanocrystals for customization to a variety of photovoltaic or photocatalytic systems.

Ordered Macroporous Supports for Pt Based Catalysis

Porous materials with a tuned loading of Pt, as well as a finely adjusted pore size and morphology of the support matrix, could enhance the mass transport efficiencies of catalyzed

reactions. A series of materials with an adjusted loading of Pt nanocrystals were prepared on ordered porous TiO_2 supports as a demonstration of a technique to directly prepare well-tuned porous catalytic supports. The resulting ordered porous TiO_2 supports exhibited a uniform surface coverage of Pt nanocrystals within these 3D matrices (Figure 3). The combination of Pt and TiO_2 can be used in a number of catalytic applications, such as methanol oxidation reactions, aldehyde and ketones hydrogenation reactions, photocatalytic hydrogen evolution, and the ORR.[57–64] The TiO_2 can exhibit an increased photocatalytic activity in the presence of Pt, reduced Pt agglomeration under high temperature conditions, and increased Pt catalytic activity by serving as a surface that promotes the adsorption of organic molecules in proximity to the Pt surfaces. [57–64] The TEM analyses of these materials indicates the formation of ordered multilayers of porous TiO_2 containing uniform and interconnected pores with an average diameter of 400 ± 40 nm. These pores were covered with a uniform coating of Pt nanocrystals (4.0 ± 0.5 nm in diameter), which were evenly spaced with an interparticle separation of 10 ± 3 nm. The high resolution TEM analysis of this material indicated the presence crystalline Pt nanocrystals with a lattice fringe spacing corresponding to the Pt (111) facet (Figure S2). The transfer of the Pt nanocrystals from the PS templates to the oxide support was further tuned to demonstrate the versatility of this preparation method. Samples were prepared with three different surface coverages of Pt nanocrystals (Figure S3). These materials were created by decorating a series of colloidal polymer templates each with a different surface coverage of Pt nanocrystals. Through the TEM analyses, the coverage of Pt nanocrystals on the polymer templates was shown to correlate with the loading of Pt nanocrystals on the TiO_2 supports (Figure S4). This result demonstrated that controlling the initial coverage of Pt nanocrystals on the pore-forming spherical templates can produce support materials with a similar and tunable

loading of Pt nanocrystals. Samples prepared with a high, medium, and low surface coverage of Pt nanocrystals were determined to have average interparticle spacings of 9 ± 2 nm, 11 ± 3 nm, and 17 ± 6 nm, respectively. These Pt loadings are higher than that achieved within a commercially available Pt/C powdered catalyst, which had an average spacing of 27 ± 7 nm between the Pt nanocrystals (Figure S5). The control over surface coverage and interparticle spacing of the Pt nanocrystals is especially important for applications that include PEMFCs and chemical sensing. For these applications the density of catalyst loading needs to be optimized for tuning localized reaction turnover rates as this influences the overall mass transport efficiencies of the corresponding reactions.[65,66] In addition, more traditional catalysts for PEMFCs prepared using Pt nanocrystals and carbon particles have been shown to easily agglomerate during the process of catalyst preparation.[67–70] This agglomeration can prevent reactants from effectively reaching all of the surfaces of these catalysts. The TEM analyses of the Pt nanocrystal coated porous supports indicated that the catalyst particles were fixed in position by the support and did not form clusters within these samples. These well-dispersed catalysts could potentially exhibit higher Pt mass activities than those with agglomeration of their catalyst particles. This lack of agglomerates in the macroporous material is attributed in part to the formation of uniform coatings of nanocrystals on the polymer templates (Figures S3 and S6). Because of the attractive interactions between the polymer template and the nanocrystals, and the electrostatic repulsion between the nanocrystals there are limited interactions that could lead to the formation of agglomerates.[71] The uniform distribution of nanocrystals on the PS templates can be further tuned by adjusting the surfactants used to stabilize both the nanocrystals and the PS colloids during the initial assembly process, such as to screen the electrostatic repulsion between individual nanocrystals.[33,62,72] This balance of interacting forces can limit the formation of

nanocrystal agglomerates on the polymeric template. It is anticipated that these finely tuned materials will have higher mass activities than commercial catalysts for PEMFCs. Platinum remains one of the optimal catalysts for PEMFC cathodes for its catalytic activity and stability.[21] It is, however, also one of the most expensive precious metals in the world.[73] The use of ordered macroporous supports for these and related nanocrystals could further optimize their utilization and reduce the overall costs for preparing catalyst materials.

Hexagonally Close-packed Arrays of Dimpled Features for Electrochemical Applications

Ordered arrays of dimpled Ni were prepared with a uniform coating of Pd nanocrystals with diameters of 13 ± 2 nm and an interparticle (edge-to-edge) spacing of 10 ± 4 nm for use in alcohol oxidation reactions. When assuming the Pd nanocrystals were immobilized onto the surface of hemispherical Ni dimples, the Pd to Ni atomic ratio was determined to be about 1:1.5. This Pd to Ni atomic ratio is within the optimal range in the literature for methanol oxidation, and could be further tuned by varying the Pd nanocrystal concentrations during the aforementioned template coating procedure.[74,75] These materials, prepared by a combination of the self-assembly processes and Ni electrodeposition, were analyzed for their catalytic efficiency towards the electrochemical oxidation of methanol. There are a number of other electrochemical reactions that also rely on nanocrystals to improve mass activity and reaction efficiency, which could benefit from these structured catalyst supports. Additional applications include the ORR, and the oxygen evolution reaction (OER). These reactions are commonly used in renewable energy generation systems, such as DMFCs, PEMFCs, and metal-air fuel cells.[76–81] Electrodeposition is a tunable process for preparing highly conductive metals of different compositions, and can be used to form a variety of 3D porous supports. Metal deposited by PVD

techniques is, in contrast, unable to coat all of the surfaces within a 3D porous support. Sophisticated techniques, such as ALD, are significantly more expensive and difficult for scaling-up the production of materials in contrast to electrodeposition techniques. An enhancement of the electrocatalytic performance of nanocrystals can also originate from the interfaces between two different materials, such as the Pd to Ni interface demonstrated herein. In the alcohol oxidation reaction, the carbon of the alcohol molecule will associate with the Pd surfaces (due to the extraordinary affinity of Pd for carbon), and the alcohol group can be readily oxidized by the neighboring oxygen rich surfaces of the electrochemically active Ni oxides. [76,82–87] Some approaches to preparing the porous supports, such as through the use of ALD, would encapsulate all of the exposed surfaces of the Pd nanocrystal. A continuous coating of Pd over the entire surface of the Ni would, however, eliminate the electrochemically exposed interfacial regions between Pd and Ni. This loss of interfacial regions can lose strong metal support interactions between the Pd and nickel oxide support, and could decrease the overall catalyst activities of these materials. The Pd nanocrystals were, therefore, transferred to the dimpled Ni surfaces using electrodeposition techniques (Figure 4). The conductive Ni support was deposited from an aqueous electrolyte solution into the interstitial spaces within the assemblies of PS spheres, which had been coated with a controlled loading of Pd nanocrystals (Figure S6). The rate of nickel deposition was finely controlled, and the thickness of the Ni support monitored to avoid covering all of the templates with Ni. For example, the surface features were tuned to approximately 2/3 and 1/2 of the height of the polymer templates as verified by FIB prepared cross-sections of the dimpled arrays (Figure S7). These arrays of dimpled Ni demonstrated the ability to fine tune the surface morphology of the catalyst support.

Arrays of Ni supported Pd nanocrystals are a relatively low cost and stable catalyst for

alcohol oxidation reactions performed under alkaline conditions.[76,82–87] The structured arrays of dimpled Ni supporting Pd nanocrystals were evaluated for their use in methanol oxidation reactions (Figure S8). A detailed description of these experiments is presented in the Electronic Supplementary Information. These experiments determined that the dimpled electrode coated with nanocrystals had a 30% higher specific activity than a planar polycrystalline Pd film (100 nm of Pd on 10 nm of Cr). At the end of the electrochemistry experiments, a cross section of the sample was prepared by FIB techniques for TEM and EDS analyses (Figure 4d). These analyses indicated that the Ni support retained the Pd nanocrystals and contained a thin surface layer of nickel oxide. This oxide layer acts as a barrier that limits the oxidation of the underlying Ni metal. This oxide layer was stable at the applied potentials required for the electrochemical oxidation of methanol. [76,82–87] This tunable templating technique could be used to prepare customized electrodes that are further optimized with regards to its overall thickness, dimensions of the pores, electrode surface morphology, and composition towards catalyzing different electrochemical alcohol oxidation reactions. It is hypothesized that similarly porous materials with a further fine-tuned pore size and surface coverage of the nanocrystals may exhibit an enhanced performance towards additional alcohol containing species. The optimization of these porous materials could be customized to account for differences in the diffusion coefficients and steric hindrance of each reaction.[88]

Randomly Assembled Nanobowls for Flow-through Catalytic Applications

Random assemblies of nanobowls, each coated with Pt nanocrystals (3 ± 1 nm in diameter) were prepared to demonstrate additional material deposition techniques commonly used on a commercial scale, such as PVD used in the production of nanostructured and/or

conductive films. Nanobowls of Au/TiO_2 (~60 nm in total thickness) supporting Pt nanocrystals were prepared, which could be easily deposited as an ink and dried as a layer with interconnecting pores for flow-through applications. One application could be for use in PEMFCs as structured catalyst layers that assist the influx and removal of fuel and products.[76–81] The pore spaces created by the curvature of the nanobowls could influence mass transport characteristics, such as to further improve the efficiency of the ORR. The sol-gel processes described herein can be easily scaled to produce commercially relevant quantities of materials. The sol-gel process is, however, most often used in the production of semiconducting or ceramic materials. The demonstrated electrodeposition techniques utilize a solution-based process, where a precise control over deposition conditions (i.e. bath concentration, circuit conductivity and impedance) is required for the formation of uniform nanometer-scale continuous thin films. Controlling these parameters for the reproduction of nanoscale features can be more challenging at commercial scales when compared to the throughput of PVD techniques.[89,90] The PVD process can be extended to create a variety of thin film materials, such as metals, metal oxides, and ceramic materials. These are scalable processes that provide an ease of controlling both material purity and thickness. Physical vapor deposition techniques can also deposit materials onto non-conductive substrates, and have been used in decal transfer and related commercial scale processes.[91] Our study utilized PVD to prepare both metal and metal oxide coatings on assemblies of nanocrystal coated PS templates. This process effectively immobilized the nanocrystals in the deposited thin films. Nanobowls were prepared with immobilized nanocrystals, which were isolated from the templates by sonication in a 50:50 (v/v) mixture of toluene and acetone. Suspensions of these nanobowls were cast as assemblies of randomly organized, 3D porous supports (Figure 5). The Au and TiO_2 multilayer compositions were chosen

in part to demonstrate the flexibility of using PVD techniques to create structures containing both metals and metal oxides that are not achievable by either sol-gel or electrodeposition alone. This material combination can also be used to prepare substrates that are active in photocatalytically induced hydrogen evolution and the ORR.[61–64,67,72,78] The Pt nanocrystals supported by these nanobowl structures were clearly identifiable in the HAADF-STEM images and EDS maps (Figures 5c and 5d). The preparation of this material demonstrated that the procedures for preparing the nanocrystal coatings on PS and their transfer to a support are compatible with commercially relevant PVD processes while retaining their nanostructured features. When compared to the other techniques demonstrated in this study, PVD techniques can be used to prepare unique nanostructures that can be further assembled into 3D structures using conventional powder processing techniques.

The results presented herein demonstrate a series of methods for creating porous and structured metals, semiconductors, and ceramic supports with tunable porosity, dimensions and compositions, as well as the ability to incorporate uniform arrays of nanocrystals. These methods can be utilized to create materials for a number of applications, such as PEMFCs, DMFCs, and dye sensitized solar cells with optimized efficiencies towards the generation of electrical energy from renewable resources, such as hydrogen, methanol, and sunlight, respectively.

Conclusions

This study has demonstrated a number of tunable approaches to preparing porous supports containing uniform coatings of nanocrystals. It was shown that the loadings of nanocrystals on spherical polymer templates can be fine-tuned with regards to the composition, size, and surface coverage of the catalyst. Subsequent procedures transferred these nanocrystals to the surfaces of a series of macroporous support materials. Different techniques to deposit or

grow the support material were used to demonstrate the preparation of materials for a range of applications. Ordered 3D macroporous supports of $Ti_{1-x}Si_xO_2$ with coatings of upconverting nanocrystals were prepared by sol-gel techniques for photocatalytic or other photonic applications. Ordered porous TiO_2 supporting uniform layers of Pt nanocrystals were prepared for catalytic reactions that include alcohol oxidation and hydrogenation reactions. By adjusting the loading of nanocrystals on the spherical polymer templates, porous TiO_2 samples were prepared with a uniform and well-tuned coverage of Pt nanocrystals. The interparticle spacing can be optimized to the specific needs of Pt based catalytic reactions. Hexagonally close-packed arrays of dimpled Ni features with Pd nanocrystal coatings were prepared for the electrochemical oxidation of alcohols. This structure exhibited higher specific current densities towards the electrochemical oxidation of methanol than planar films of polycrystalline Pd. Nanobowls containing a multilayer of Au and TiO_2 coated with Pt nanocrystals were prepared by PVD techniques and assembled into randomly packed 3D structures to demonstrate an extension of these techniques to relevant commercial processes for producing nanostructured materials for fuel cell applications. The use of these modular techniques can be utilized to produce nanostructured materials with a tunable porosity and structure, as well as finely adjusted nanocrystal loadings and catalysts-support interactions for enhancing chemical, electrochemical, and photochemical processes. The ability to tune each of these properties can increase the catalytic efficiency and stability of the nanocrystals, optimize the utilization of the nanocrystals, create synergistic effects at disparate interfaces, and reduce consumption of precious metals and other valuable materials.

Funding Sources

Financial support for this work was provided by the Natural Sciences and Engineering Research Council (NSERC) of Canada Discovery Program (Grant No. 1077758), CMC Microsystems (MNT Grant No. 2152), Canada Research Chairs Program (B.D. Gates; Grant No. 950-215846), and the Engineered Nickel Catalysts for Electrochemical Clean Energy project administered from Queen's University and supported in part by Grant No. RGPNM 477963-2015 from the NSERC of Canada Discovery Frontiers Program. This work made use of 4D LABS (www.4dlabs.ca) and the Centre for Soft Materials shared facilities supported by the Canada Foundation for Innovation (CFI), British Columbia Knowledge Development Fund (BCKDF), Western Economic Diversification Canada, and Simon Fraser University.

Conflicts of interest

There are no conflicts to declare.

Acknowledgements

We would like to thank Mr. Austin (Woo hyuk) Lee for performing physical vapor deposition of Au and TiO_2 thin films, and Dr. John-Christopher Boyer for providing the $NaYF_4$ nanocrystals for use in this study.

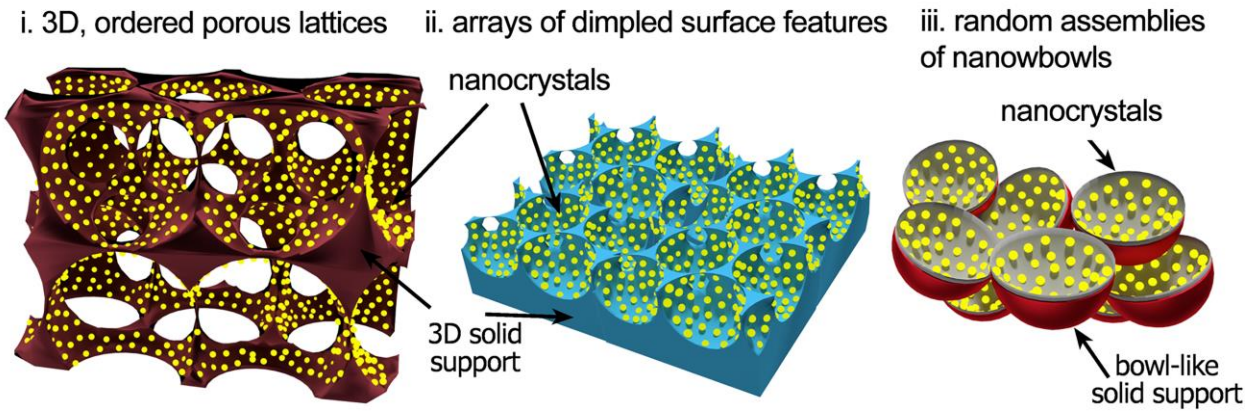

Figure 1. Schematic depictions of three approaches to preparing nanocrystal coated supports: (i) an ordered 3D porous lattice; (ii) a 2D array of dimpled features with a tunable surface roughness; and (iii) a lattice assembled from nanobowls.

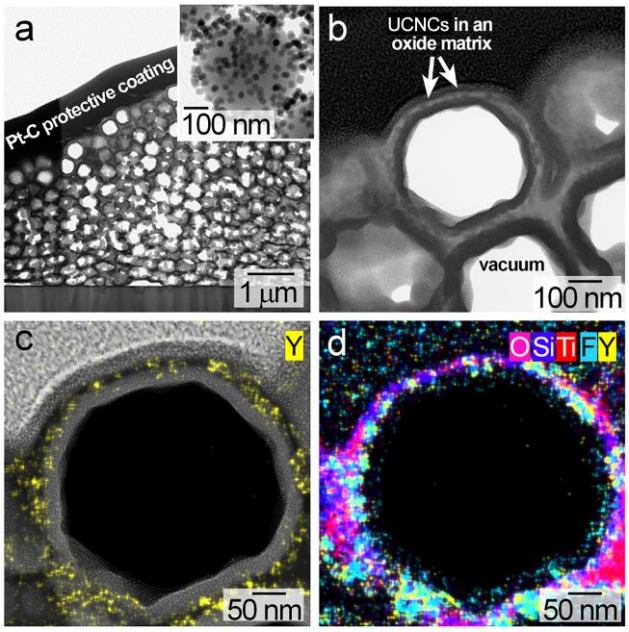

Figure 2. Transmission electron microscopy (TEM) analyses of $NaYF_4$ upconverting nanocrystals (UCNCs) with a diameter (ø) of 26 ± 4 nm that were transferred from spherical polystyrene templates into a porous metal oxide lattice with a pore ø of 320 ± 30 nm. (a) Bright field Scanning TEM (STEM) image of a section of this porous structure prepared by focused ion beam (FIB) assisted lift-out; (a, inset) UCNCs loaded onto the colloidal polystyrene templates. (b) High magnification STEM image from a section of the sample in (a) depicting the $NaYF_4$ nanocrystals within the metal oxide support. (c) An energy dispersive X-ray spectroscopy (EDS) map of yttrium overlapped on a high angle annular dark field (HAADF) STEM image to depict the locations of the $NaYF_4$ nanocrystals within the support matrix. (d) Overlapping EDS maps of the majority of elements present in the nanostructured support (i.e. Na is excluded from this map).

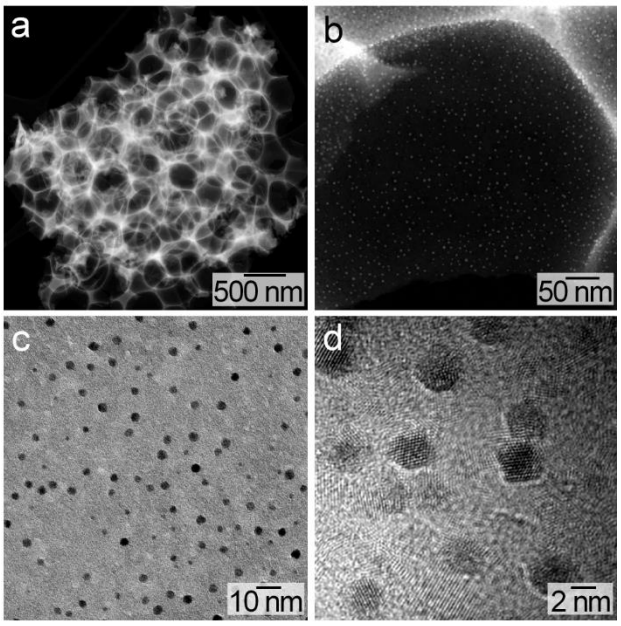

Figure 3. Transmission electron microscopy and STEM images of Pt nanocrystals (ø = 3.4 ± 0.5 nm) supported on a porous frame work of TiO_2 (ø = 400 ± 38 nm): (a) HAADF-STEM image of a section of the nanostructured support; (b) a higher magnification HAADF-STEM image from a region in (a) depicting the Pt nanocrystals supported on the titania; (c) higher magnification bright field TEM image of the same sample; and (d) high resolution TEM (HRTEM) image depicting lattice fringes of the Pt nanocrystals on the TiO_2 support. See Figure S2 for a detailed analysis of the lattice fringes in the high resolution TEM images.

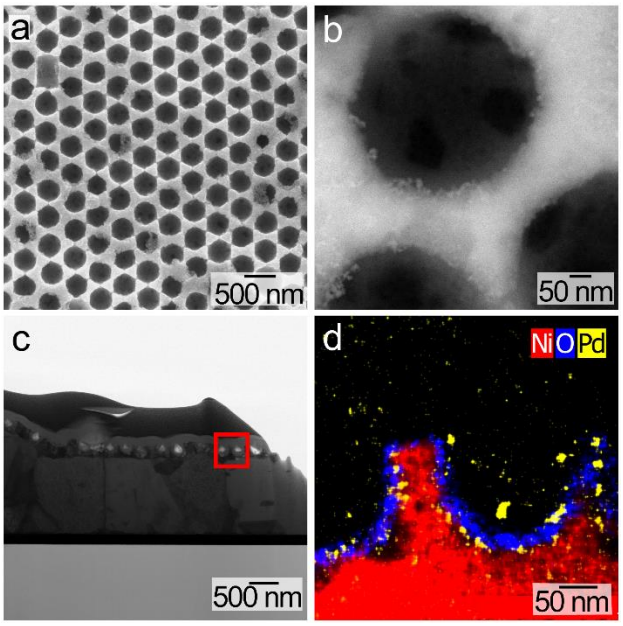

Figure 4. Scanning electron microscopy (SEM) and TEM images of Pd nanocrystals (ø = 13 ± 2 nm) supported within an array of dimpled Ni features with a periodicity of ~340 nm: (a) lower magnification image obtained using a secondary electron detector (SED) to analyze the array of close-packed features within the dimpled Ni; (b) higher magnification image using a concentric backscattered electron detector indicating the presence of Pd nanocrystals on the Ni surfaces as visualized by the contrast in electron density of these elements; and (c) bright field STEM image from a section of the sample prepared by FIB milling and lift-out. The red box in (c) indicates the location associated with (d), which depicts the EDS combined elemental maps confirming the presence of Pd nanocrystals on the surfaces of the structured Ni support.

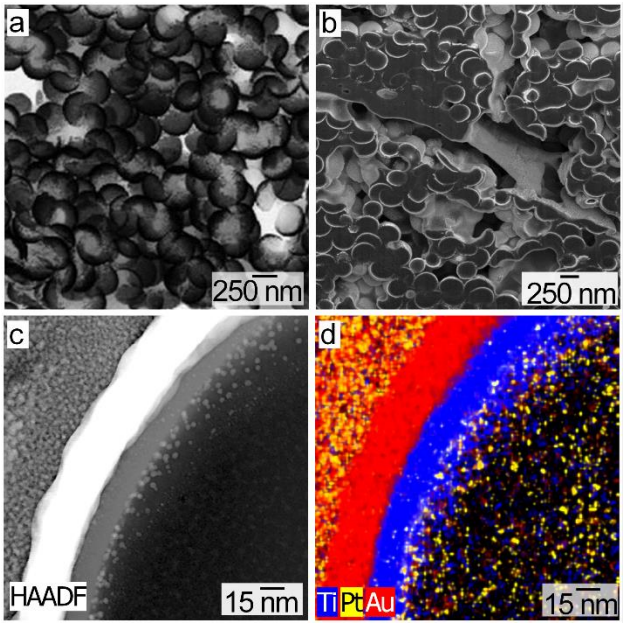

Figure 5. Scanning electron microscopy and TEM images of Pt nanocrystals (ø = 2.8 ± 0.5 nm) supported on the surfaces of nanobowls prepared from a composite of Au and TiO_2 (ø = ~350 nm): (a) bright field TEM image of the Pt nanocrystals supported on a randomly assembled structure prepared from these nanobowls; (b) SEM image collected using a SED of a FIB prepared cross-section of the same sample of nanobowls that was also mixed with a DuPont™ DE2020 ionomer; (c) HAADF-STEM image from a cross-section of a single nanoshell; and (d) combined image of the Ti, Pt, and Au EDS elemental maps for the nanostructure shown in (c).

References

1 F. Raimondi, G. G. Scherer, R. Kötz and A. Wokaun, *Angew. Chemie - Int. Ed.*, 2005, 44, 2190–2209.

2 A. S. Aricò, P. Bruce, B. Scrosati, J.-M. Tarascon and W. van Schalkwijk, *Nat. Mater.*, 2005, **4**, 366–377.

3 C. Liu, U. Burghaus, F. Besenbacher and Z. L. Wang, *ACS Nano*, 2010, **4**, 5517–5526.

4 O. Antoine, Y. Bultel and R. Durand, *J. Electroanal. Chem.*, 2001, **499**, 85–94.

5 Z. P. Sun, X. G. Zhang, Y. Y. Liang and H. L. Li, *Electrochem. Commun.*, 2009, **11**, 557–561.

6 P. Waszczuk, J. Solla-Gullón, H.-S. Kim, Y. Y. Tong, V. Montiel, A. Aldaz and A. Wieckowski, *J. Catal.*, 2001, **203**, 1–6.

7 A. J. Nozik, *Nano Lett.*, 2010, **10**, 2735–2741.

8 N. Johnson, D. McComb, A. Richel, B. Treble and R. De La Rue, *Synth. Met.*, 2001, **116**, 469–473.

9 R. C. Schroden, M. Al-Daous, C. F. Blanford and A. Stein, *Chem. Mater.*, 2002, **14**, 3305–3315.

10 B. Kinkead, J. van Drunen, M. T. Y. Paul, K. Dowling, G. Jerkiewicz and B. D. Gates, *Electrocatalysis*, 2013, **4**, 179–186.

11 O.-H. Kim, Y.-H. Cho, S. H. Kang, H.-Y. Park, M. Kim, J. W. Lim, D. Y. Chung, M. J. Lee, H. Choe and Y.-E. Sung, *Nat. Commun.*, 2013, **4**, 2473.

12 M. T. Y. Paul, B. Kinkead and B. D. Gates, *J. Electrochem. Soc.*, 2014, **161**, B3103–B3106.

13 Y. Lei, J. Lu, X. Luo, T. Wu, P. Du, X. Zhang, Y. Ren, J. Wen, D. J. Miller, J. T. Miller, Y. K. Sun, J. W. Elam and K. Amine, *Nano Lett.*, 2013, **13**, 4182–4189.

14 N. V. Long, C. M. Thi, M. Nogami and M. Ohtaki, *New J. Chem.*, 2012, **36**, 1320–1334.

15 B. K. Pilapil, J. van Drunen, Y. Makonnen, D. Beauchemin, G. Jerkiewicz and B. D. Gates, *Adv. Funct. Mater.*, 2017, **27**, 10703171

16 A. Lewera, L. Timperman, A. Roguska and N. Alonso-Vante, *J. Phys. Chem. C*, 2011, **115**, 20153–20159.

17 W. Luc and F. Jiao, *Acc. Chem. Res.*, 2016, **49**, 1351–1358.

18 F. Maillard, S. Schreier, M. Hanzlik, E. R. Savinova, S. Weinkauf and U. Stimming, *Phys. Chem. Chem. Phys.*, 2005, **7**, 385–393.

19 M. H. Park, K. Kim, J. Kim and J. Cho, *Adv. Mater.*, 2010, **22**, 415–418.

20 T. Teranishi, M. Hosoe, T. Tanaka and M. Miyake, *J. Phys. Chem. B*, 1999, **103**, 3818–3827.

21 R. Latsuzbaia, E. Negro and G. Koper, *Fuel Cells*, 2015, **15**, 628–638.

22 N. Saibuathong, Y. Saejeng, K. Pruksathorn, M. Hunsom and N. Tantavichet, *Journal of Applied Electrochemistry*, 2010, **40**, 903–910.

23 C. R. K. Rao and D. C. Trivedi, *Coord. Chem. Rev.*, 2005, **249**, 613–631.

24 Y.-C. Hsueh, C.-C. Wang, C.-C. Kei, Y.-H. Lin, C. Liu and T.-P. Perng, *J. Catal.*, 2012, **294**, 63–68.

25 B. M. E. Baumgartner and C. J. Raub, *Platin. Met. Rev.*, 1988, **32**, 188–197.

26 J. Ustarroz, T. Altantzis, J. A. Hammons, A. Hubin, S. Bals and H. Terryn, *Chem. Mater.*, 2014, **26**, 2396–2406.

27 B. Geboes, B. Vanrenterghem, J. Ustarroz and D. Pauwels, *Chem. Eng. Trans.*, 2014, **41**, 73–78.

28 I. Lee, Q. Zhang, J. Ge, Y. Yin and F. Zaera, *Nano Res.*, 2011, **4**, 115–123.

29 K. Sasaki, L. Zhang and R. R. Adzic, *Phys. Chem. Chem. Phys.*, 2008, **10**, 159–167.

30 M. Wen, B. Zhou, H. Fang, Q. Wu and S. Chen, *J. Phys. Chem. C*, 2014, **118**, 26713–26720.

31 J. M. Lee, Y. D. Jun, D. W. Kim, Y. H. Lee and S. G. Oh, *Mater. Chem. Phys.*, 2009, **114**, 549–555.

32 A. Dokoutchaev, J. T. James, S. C. Koene, S. Pathak, G. K. S. Prakash and M. E. Thompson, *Chem. Mater.*, 1999, **11**, 2389–2399.

33 B. K. Pilapil, M. C. P. Wang, M. T. Y. Paul, A. Nazemi and B. D. Gates, *Nanotechnology*, 2015, **26**, 55601.

34 A. A. Zakhidov, *Science*, 1998, **282**, 897–901.

35 Z. Zhong, Y. Yin, B. Gates and Y. Xia, *Adv. Mater.*, 2000, **12**, 206–209.

36 K. Kim, P. Thiyagarajan, H.-J. Ahn, S.-I. Kim and J.-H. Jang, *Nanoscale*, 2013, **5**, 6254–60.

37 T. Teranishi, R. Kurita and M. Miyake, *J. Inorg. Organomet. Polym.*, 2000, **10**, 145–156.

38 T. Teranishi and M. Miyake, *Chem. Mater.*, 1998, **10**, 594–600.

39 J. C. Boyer, F. Vetrone, L. A. Cuccia and J. A. Capobianco, *J. Am. Chem. Soc.*, 2006, **128**, 7444–7445.

40 A. Blanco, E. Chomski, S. Grabtchak, M. Ibisate, S. John, S. Leonard, C. Lopez, F. Meseguer, H. Miguez, J. Mondia, G. Ozin, O. Toader and H. M.van Driel, *Nature*, 2000, **405**, 437–40.

41 B. Kinkead, J. van Drunen, M. T. Y. Paul, K. Dowling, G. Jerkiewicz and B. D. Gates, *Electrocatalysis*, 2013, **4**, 179–186.

42 J. Van Drunen, B. K. Pilapil, Y. Makonnen, D. Beauchemin, B. D. Gates and G. Jerkiewicz, *ACS Appl. Mater. Interfaces*, 2014, **6**, 12046–12061.

43 Y. Xia, B. Gates, Y. Yin and Y. Lu, *Adv. Mater.*, 2000, **12**, 693–713.

44 A. Van Blaaderen, *Nature*, 2006, 439, 545–546.

45 S. A. Asher, J. Holtz, L. Liu and Z. Wu, *J. Am. Chem. Soc.*, 1994, **116**, 4997–4998.

46 G. M. Whitesides, *Science*, 2002, **295**, 2418–2421.

47 P. Colson, R. Cloots and C. Henrist, *Langmuir*, 2011, **27**, 12800–12806.

48 X. Ma and X. Ni, *J. Nanocrystal Res.*, 2013, **15**, 1-7.

49 G. F. Álvarez, M. Mamlouk and K. Scott, *Int. J. Electrochem.*, 2011, **2011**, 1–12.

50 F. Zhang, C. L. Zhang, H. Y. Peng, H. P. Cong and H. S. Qian, *Part. Part. Syst. Charact.*, 2016, **9**, 248–253.

51 F. Zhang, C. L. Zhang, W. N. Wang, H. P. Cong and H. S. Qian, *Chem. Sus. Chem.*, 2016, **9**, 1449–1454.

52 X. Guo, W. Di, C. Chen, C. Liu, X. Wang and W. Qin, *Dalton Trans.*, 2014, **43**, 1048–54.

53 W. Wang, Y. Li, Z. Kang, F. Wang and J. C. Yu, *Appl. Catal. B Environ.*, 2016, **182**, 184–192.

54 Q. Lü, L.-C. Zhao, F.-Y. Guo and M.-C. Li, *Chinese Phys. B*, 2009, **18**, 4030–4036.

55 J. Yu, Y. Yang, R. Fan, D. Liu, L. Wei, S. Chen, L. Li, B. Yang and W. Cao, *Inorg. Chem.*, 2014, **53**, 8045–8053.

56 F. Priolo, T. Gregorkiewicz, M. Galli and T. F. Krauss, *Nat. Nanotechnol.*, 2014, **9**, 19–32.

57 I. S. Cho, C. H. Lee, Y. Feng, M. Logar, P. M. Rao, L. Cai, D. R. Kim, R. Sinclair and X. Zheng, *Nat. Commun.*, 2013, **4**, 1723.

58 R. Su, R. Tiruvalam, A. J. Logsdail, Q. He, C. A. Downing, M. T. Jensen, N. Dimitratos, L. Kesavan, P. P. Wells, R. Bechstein, H. H. Jensen, S. Wendt, C. R. A. Catlow, C. J. Kiely, G. J. Hutchings and F. Besenbacher, *ACS Nano*, 2014, **8**, 3490–3497.

59 M. A. Barakat, R. I. Al-Hutailah, E. Qayyum, J. Rashid and J. N. Kuhn, *Environ. Technol.*, 2014, **35**, 137–44.

60 B. L. An, Y. H. Fu, F. Z. Dai and J. Q. Xu, *J. Alloys Compd.*, 2015, **622**, 426–431.

61 X. Li, W. Zheng, H. Pan, Y. Yu, L. Chen and P. Wu, *J. Catal.*, 2013, **300**, 9–19.

62 Y. Y. Song, Z. Da Gao and P. Schmuki, *Electrochem. Commun.*, 2011, **13**, 290–293.

63 J. Yu, L. Qi and M. Jaroniec, *J. Phys. Chem. C*, 2010, **114**, 13118–13125.

64 J. J. Zou, H. He, L. Cui and H. Y. Du, *Int. J. Hydrogen Energy*, 2007, **32**, 1762–1770.

65 J. P. Owejan, J. E. Owejan and W. Gu, *J. Electrochem. Soc.*, 2013, **160**, F824–F833.

66 C. Liewhiran, N. Tamaekong, A. Tuantranont, A. Wisitsoraat and S. Phanichphant, *Mater. Chem. Phys.*, 2014, **147**, 661–672.

67 A. López-Cudero, J. Solla-Gullón, E. Herrero, A. Aldaz and J. M. Feliu, *J. Electroanal. Chem.*, 2010, **644**, 117–126.

68 J. E. Newton, J. A. Preece and B. G. Pollet, *Int. J. Low-Carbon Technol.*, 2011, **7**, 38-43.

69 M. Chen and Y. Xing, *Langmuir*, 2005, **21**, 9334–9338.

70 K. Yoshii, T. Tsuda, T. Arimura, A. Imanishi, T. Torimoto and S. Kuwabata, *RSC Adv.*, 2012, **2**, 8262.

71 W. Qian, W. Zhaoqun, K. Xuanfeng, G. Xiaodan and X. Gi, *Langmuir*, 2008, **24**, 7778–7784.

72 Z. Zhang, Z. Wang, S. W. Cao and C. Xue, *J. Phys. Chem. C*, 2013, **117**, 25939–25947.

73 E. J. Carlson, P. Kopf, J. Sinha, S. Sriramulu and Y. Yang, *Natl. Renew. Energy Lab.*, 2005, NREL/SR-560-39104.

74 L. Chen, L. Lu, H. Zhu, Y. Chen, Y. Huang, Y. Li and L. Wang, *Nat. Commun.*, 2017, **8**, 14136.

75 J. Calderón, M. Rios Ráfales, M. Nieto-Monge, J. Pardo, R. Moliner and M. Lázaro, *Nanomaterials*, 2016, **6**, 187.

76 R. N. Singh, A. Singh and Anindita, *Int. J. Hydrogen Energy*, 2009, **34**, 2052–2057.

77 J. X. Wang, H. Inada, L. Wu, Y. Zhu, Y. Choi, P. Liu, W. P. Zhou and R. R. Adzic, *J. Am. Chem. Soc.*, 2009, **131**, 17299–17302.

78 Y. Mu, H. Liang, J. Hu, L. Jiang and L. Wan, *J. Phys. Chem. B*, 2005, **109**, 22212–22216.

79 Z. Zhang, L. Xin, K. Sun and W. Li, *Int. J. Hydrogen Energy*, 2011, **36**, 12686–12697.

80 W. Hou, N. A. Dehm and R. W. J. Scott, *J. Catal.*, 2008, **253**, 22–27.

81 C. Xu, H. Wang, P. K. Shen and S. P. Jiang, *Adv. Mater.*, 2007, **19**, 4256–4259.

82 A. Manzo-Robledo, N. J. S. Costa, K. Philippot, L. M. Rossi, E. Ramírez-Meneses, L. P. A. Guerrero-Ortega and S. Ezquerra-Quiroga, *J. Nanocrystal Res.*, 2015, **17**, 1–8.

83 M. D. Obradović, Z. M. Stančić, U. Lačnjevac, V. V. Radmilović, A. Gavrilović-Wohlmuther, V. R. Radmilović and S. L. Gojković, *Appl. Catal. B Environ.*, 2016, **189**, 110–118.

84 C. Qiu, R. Shang, Y. Xie, Y. Bu, C. Li and H. Ma, *Mater. Chem. Phys.*, 2010, **120**, 323–330.

85 M. Zhang, Z. Yan and J. Xie, *Electrochim. Acta*, 2012, **77**, 237–243.

86 Z. Qi, H. Geng, X. Wang, C. Zhao, H. Ji, C. Zhang, J. Xu and Z. Zhang, *J. Power Sources*, 2011, **196**, 5823–5828.

87 Y. Zhao, X. Yang, J. Tian, F. Wang and L. Zhan, *Int. J. Hydrogen Energy*, 2010, **35**, 3249–3257.

88 J. González-Cobos, S. Baranton and C. Coutanceau, *J. Phys. Chem. C*, 2016, **120**, 7155–7164.

89 J. Rymarczyk and D. Piotr, *Polish Journal of Chemical Technology*, 2014, **16** 18–24.

90 G. Zangari, *Coatings*, 2015, **5**, 195–218.

91 W. R. Childs and R. G. Nuzzo, *J. Am. Chem. Soc.*, 2002, **124**, 13583–13596.